

Electronic Supplementary Information

In Situ Growth of POMOFs and Derived Nitride on Cu Foam to Produce Hydrogen with Promoted Water Dissociation Kinetics

Yu-Jia Tang,^{a,b,#} Yu Wang,^{c,#} Hong-Jing Zhu,^a Kun Zhou,^{b,c,*} and Ya-Qian Lan^{a,*}

a. Jiangsu Collaborative Innovation Centre of Biomedical Functional Materials, Jiangsu Key Laboratory of New Power Batteries, School of Chemistry and Materials Science, Nanjing Normal University, Nanjing 210023, China

b. School of Mechanical and Aerospace Engineering, Nanyang Technological University, 50 Nanyang Avenue, Singapore 639798, Singapore

c. Environmental Process Modelling Centre, Nanyang Environment and Water Research Institute, Nanyang Technological University, 1 CleanTech Loop, Singapore 637141, Singapore

#These authors contributed equally to this work

*To whom all correspondence should be addressed

Corresponding Author

yqlan@njnu.edu.cn; kzhou@ntu.edu.sg

Computational details.

We constructed several periodic surface slabs to investigate the HER activity origin. Briefly, a Cu slab, four-layer (3×3) Cu (111) plane, was modeled to represent the active surface Cu in Cu-NC/CF. For the active part of MoN-Cu-NPC/CF, a hybrid MoN-Cu slab was utilized, which was a heterogeneous structure consisting of a four-layer (2×2) MoN (001) plane slab in the bottom and a single-layer ($\sqrt{19} \times \sqrt{19}$) Cu (111) plane in the top. Note that the lattice mismatch for this heterogeneous slab was as small as 0.7%. Moreover, a sole MoN slab, six-layer ($\sqrt{3} \times \sqrt{3}$) MoN (001) plane, was considered to study the role of MoN part. For all slabs, the vacuum space was kept to be larger than 16 Å to keep the image interaction negligible. The dipole correction was included during the atomic position optimization. The free energy of adsorbed H (ΔG_H) on the slabs was expressed as:

$$\Delta G_H = \Delta E_H + \Delta E_{ZPE} - T\Delta S$$

where ΔE_H was the hydrogen adsorption energy, ΔE_{ZPE} and ΔS were the difference of zero point energy (E_{ZPE}) and entropy (S), respectively, and T was the system temperature (298.15 K). For H*, E_{ZPE} and S were obtained by the vibrational frequencies calculations with harmonic vibrational motions with neglecting contributions from slab, whereas for H₂, these were taken from the NIST database. The related contributions to G are summarized in **Table S3**.

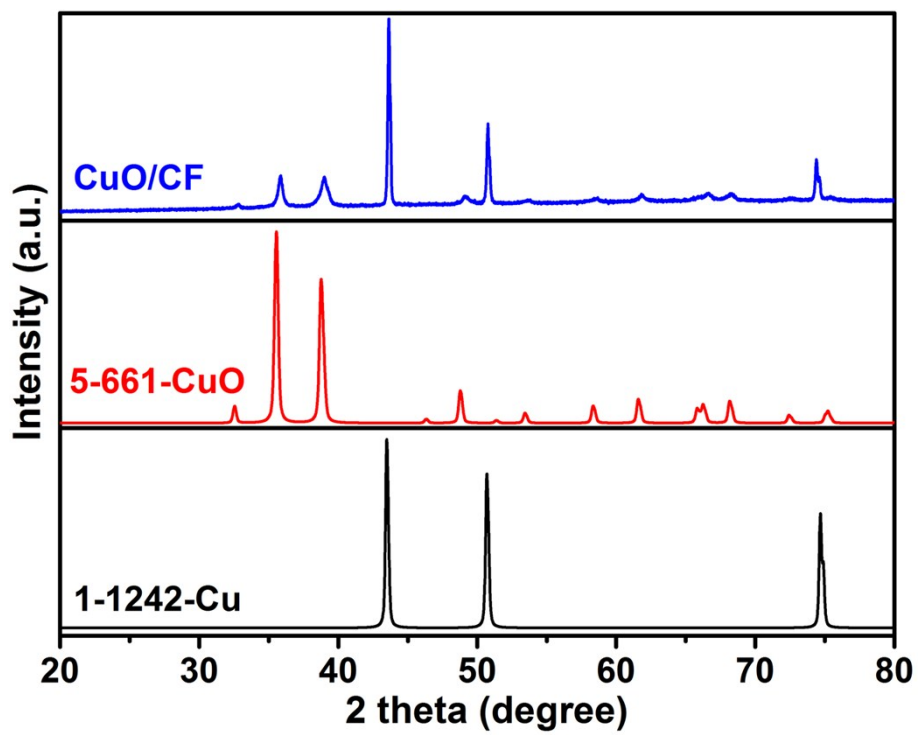


Figure S1. XRD spectrum of the oxidized CF.

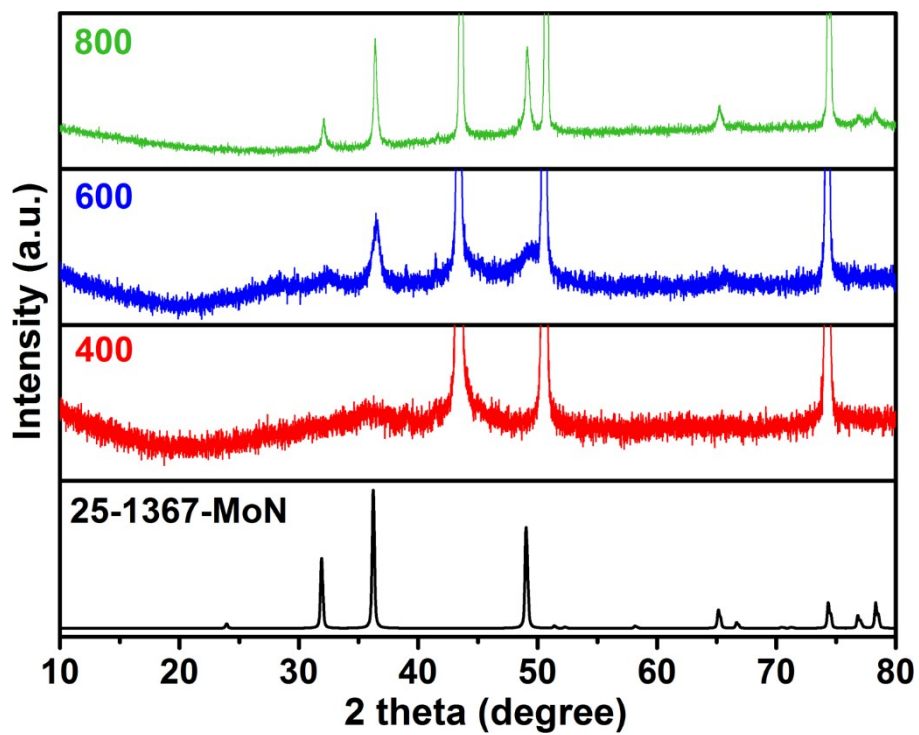


Figure S2. PXRD spectra of MoN-Cu-NPC/CF prepared at different ammoniation temperatures (400, 600 and 800 °C).

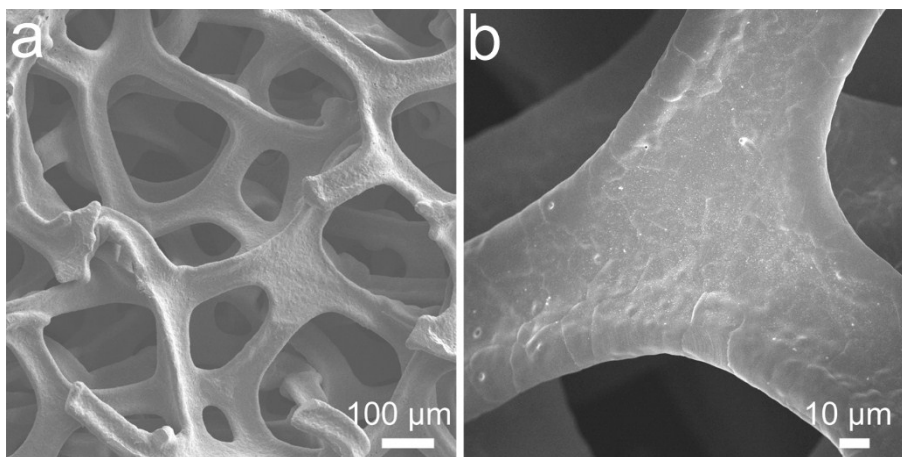
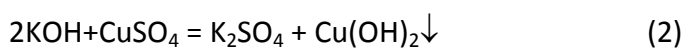
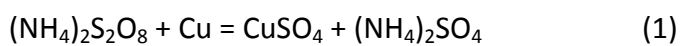


Figure S3. (a, b) SEM images of bare Cu foam at different scales.

The Cu foam showed smooth surface. After oxidation treatment, the Cu foam exhibited the rough surface because the CuO nanosheets are formed densely on its skeleton.^{1,2}

The relevant reaction equations (1), (2) and (3) are as follows:



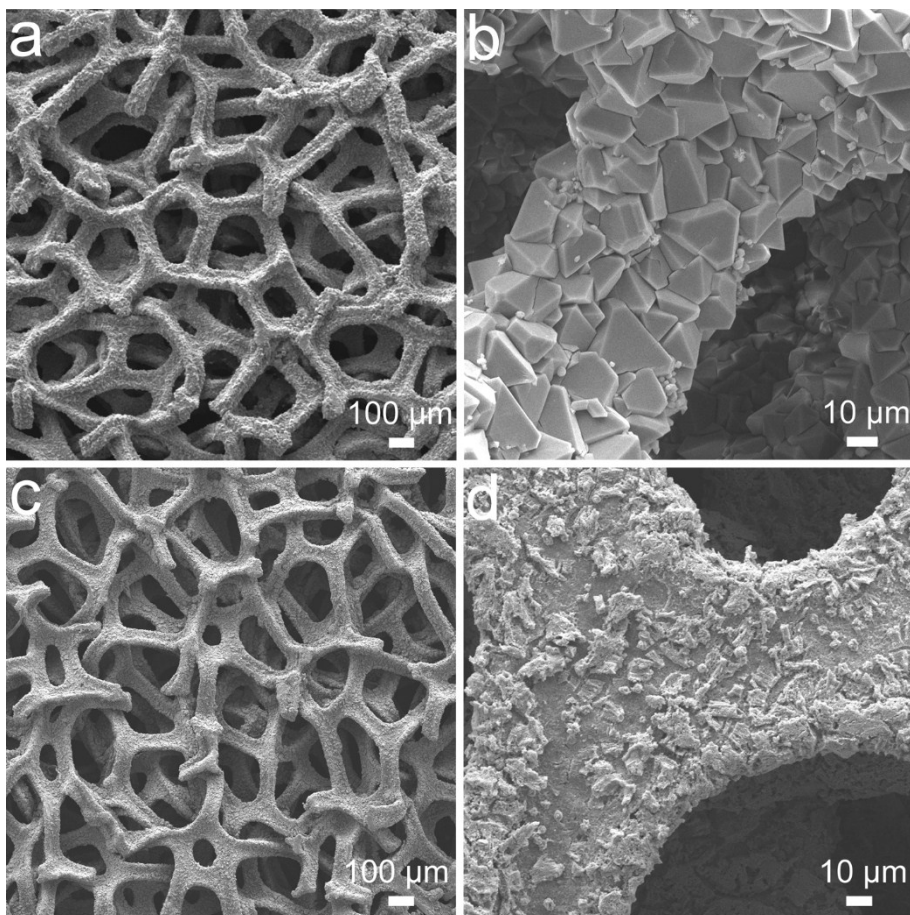


Figure S4. SEM images of (a, b) HKUST-1/CF and (c, d) Cu-NC/CF at different scales.

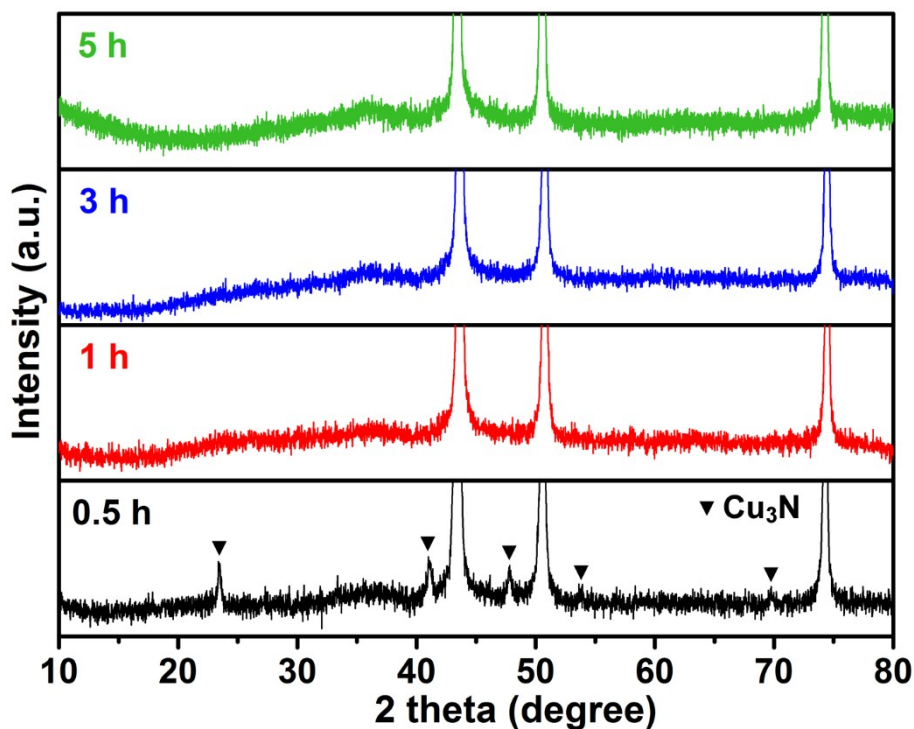


Figure S5. PXR D spectra of MoN-Cu-NPC/CF obtained at the different ammoniation time intervals (0.5, 1, 3 and 5 h).

Different ammoniation time intervals were chosen to observe the minute changes of compositions and morphologies for MoN-Cu-NPC/CF. As the ammoniation time increased, the PXR D spectra show that the peak intensity at 36.3° gradually increased, suggesting the formation of MoN. A new species of Cu_3N (JCPDS No. 86-2283) formed in 0.5 h and then disappeared. Cu_3N could be formed quickly by the reaction of NH_3 and Cu at the low annealing temperature (less than 400°C). However, Cu_3N showed poor thermal stability at NH_3 atmosphere and decomposed with increasing ammoniation time and high temperature.^{3,4} Therefore, the final compositions of MoN-Cu-NPC/CF were MoN and Cu.

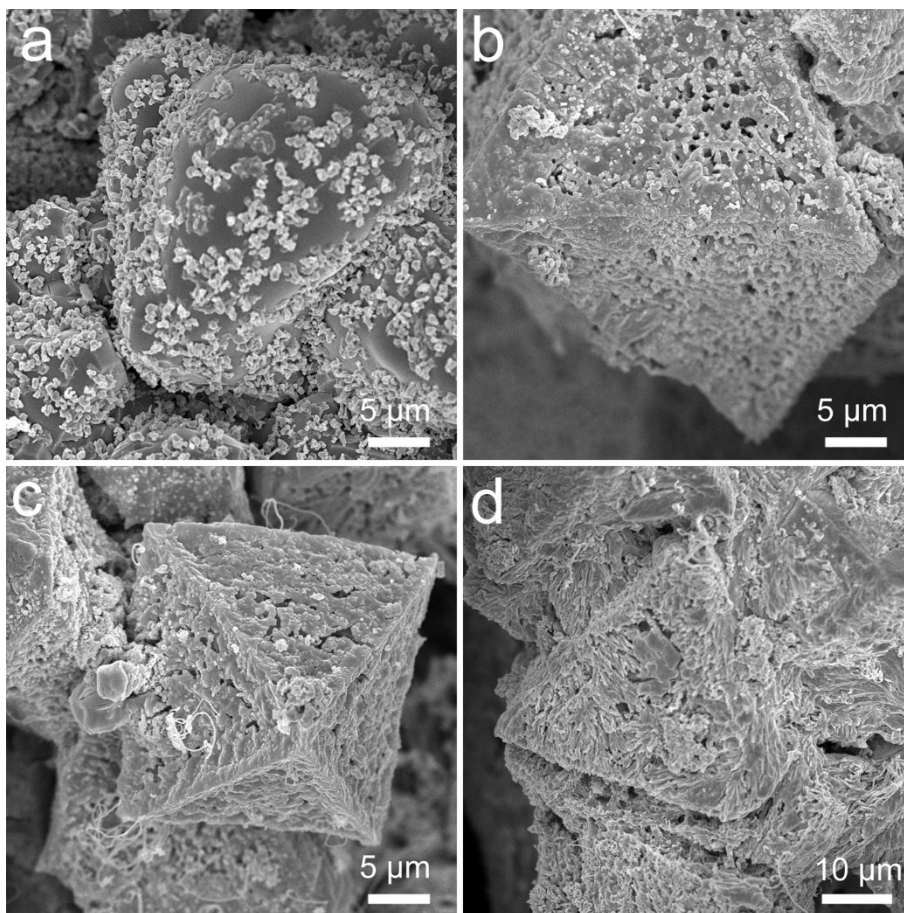


Figure S6. SEM images of MoN-Cu-NPC/CF obtained at different ammoniation time intervals: (a) 0.5 h, (b) 1 h, (c) 3 h and (d) 5 h.

In 0.5 h, the SEM image shows that the small particles were grown on the surface of $\text{PMo}_{12}\text{@HKUST-1}$ precursor, indicating the formation of Cu_3N . As the ammoniation time increased (1, 3, and 5 h), the $\text{PMo}_{12}\text{@HKUST-1}$ precursor with smooth surface gradually decomposed to become rough and wrinkled, which was the result of the reaction of NH_3 with POMOFs.

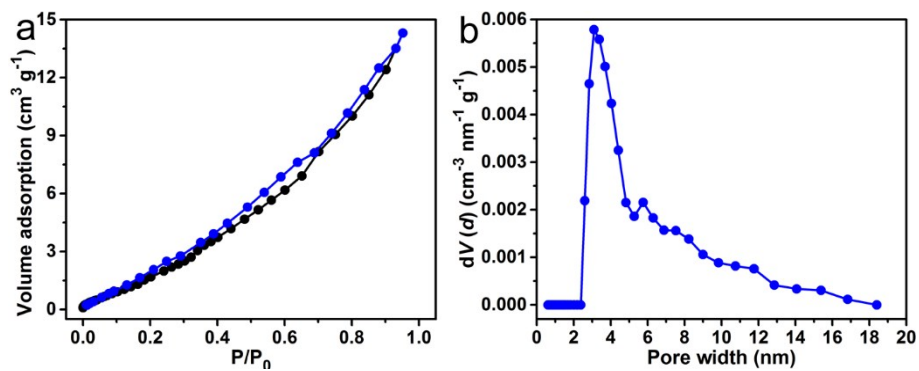


Figure S7. (a) N_2 adsorption-desorption isotherm of MoN-Cu-NPC/CF. (b) Pore size distribution curve fitted through QSDFT equilibrium model.

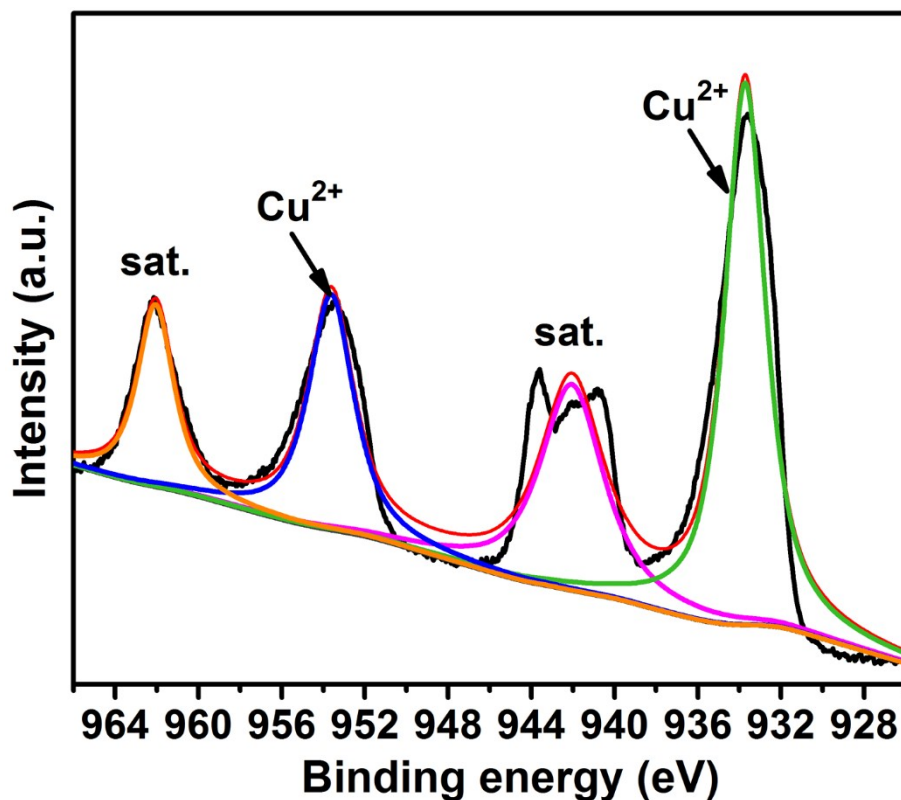


Figure S8. High-resolution Cu 2p XPS spectrum of the oxidized CF.

The high-resolution Cu 2p XPS spectrum shows that both of the two prominent peaks located at 953.6 and 933.7 eV were assigned to Cu(II) derived from CuO species. Other two peaks located at 962.1 and 942.2 eV were the corresponding satellite peaks.

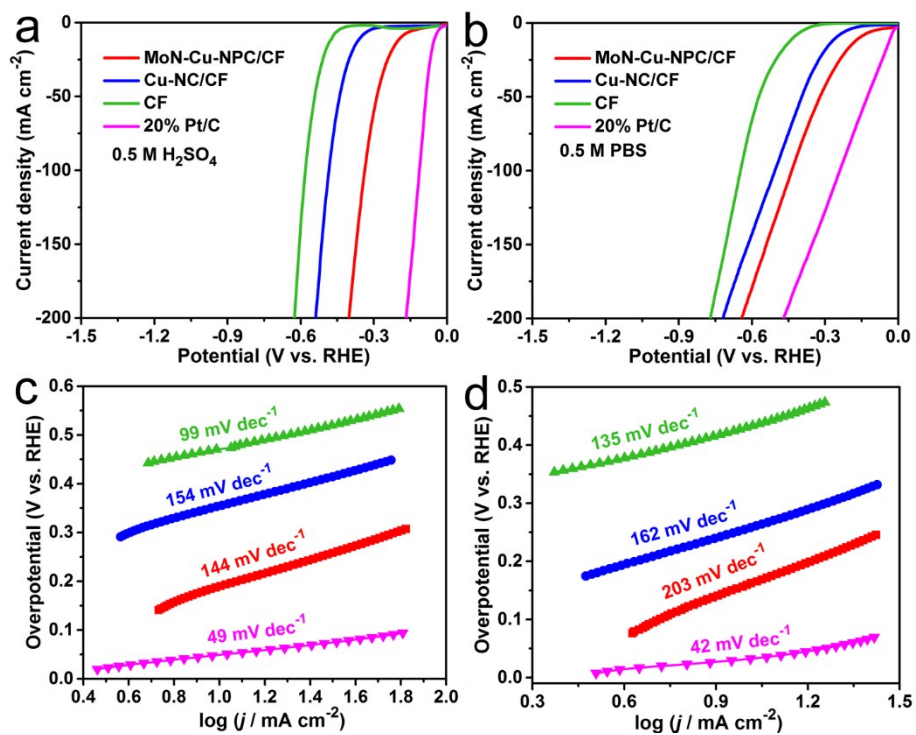


Figure S9. LSV curves of MoN-Cu-NPC/CF, Cu-NC/CF, CF and commercial 20% Pt/C in (a) 0.5 M H₂SO₄ and (b) 0.5 M PBS at 5 mV s⁻¹. Corresponding Tafel plots in (c) 0.5 M H₂SO₄ and (d) 0.5 M PBS.

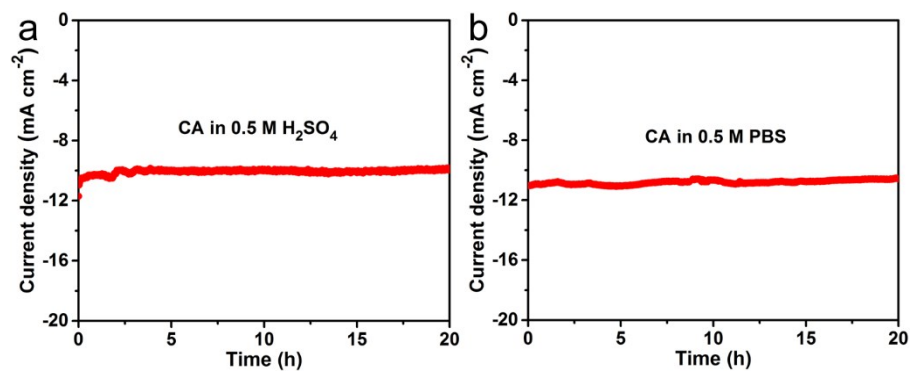


Figure S10. Chronoamperometry curves of MoN-Cu-NPC/CF performed at a constant overpotential for 20 h in (a) 0.5 M H₂SO₄ and (b) 0.5 M PBS.

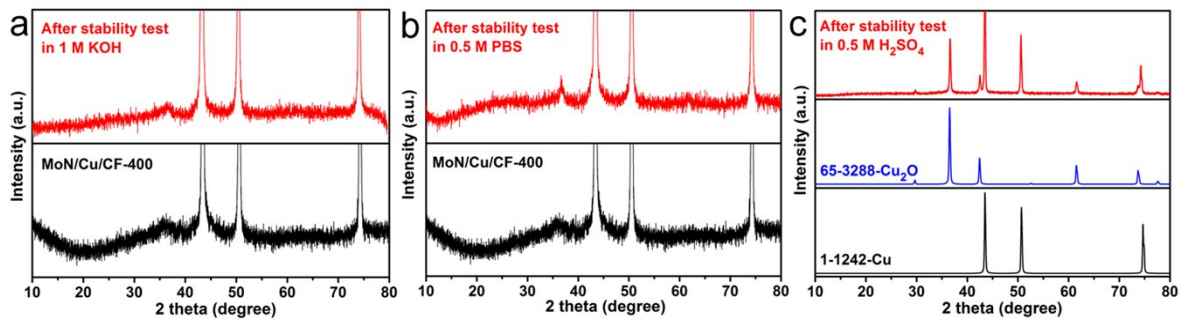


Figure S11. PXRD spectra of MoN-Cu-NPC/CF electrode after stability test in: (a) 1 M KOH, (b) 0.5 M PBS and (c) 0.5 M H₂SO₄.

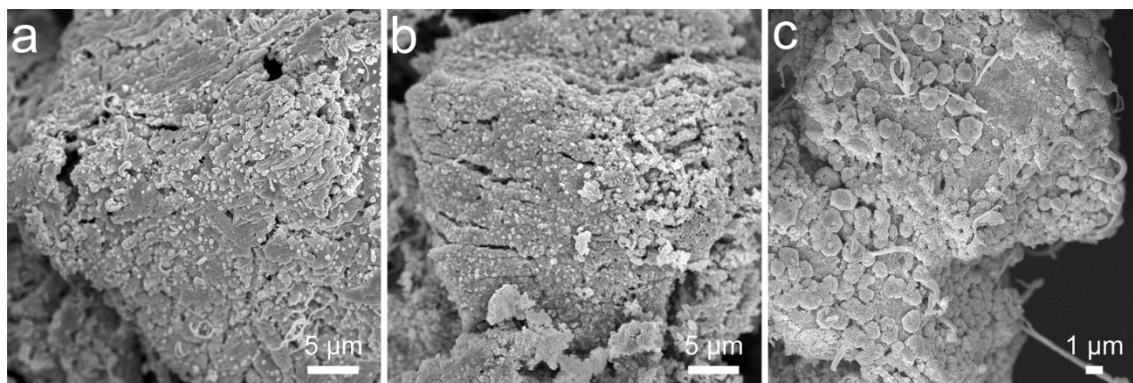


Figure S12. SEM images of MoN-Cu-NPC/CF electrode after stability test in: (a) 1 M KOH, (b) 0.5 M PBS and (c) 0.5 M H₂SO₄.

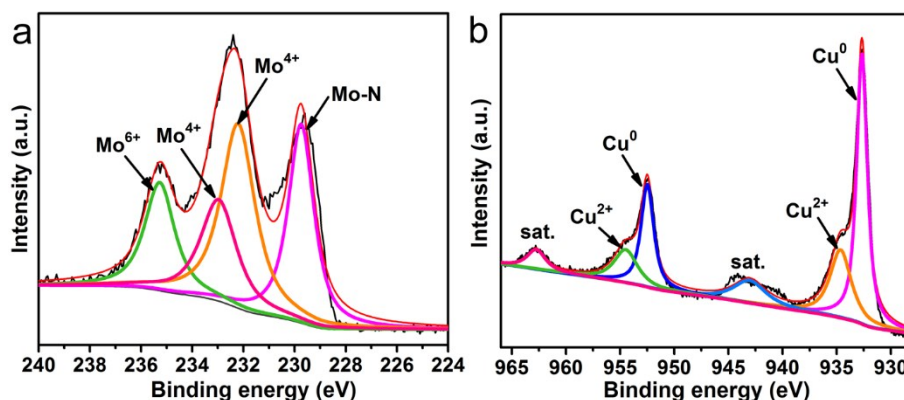


Figure S13. High-resolution XPS spectra of MoN-Cu-NPC/CF electrode after stability test in 1 M KOH: (a) Cu 2p and (b) Mo 3d.

A series of the post characterizations (*i.e.*, PXRD, SEM and XPS) were applied to study the composition and morphology of MoN-Cu-NPC/CF after long-term stability test (1000 CV cycles) in all-pH-values electrolytes.

First, the PXRD spectra of MoN-Cu-NPC/CF electrode after stability test in basic and neutral electrolytes matches well with the initial one, indicating no chemical changes as well as the high stability. In contrast, the Cu₂O (JPCDS No. 65-3288) was newly formed after stability test due to the possible electrodeposition of CF in the acidic electrolyte.⁵

Then, the SEM images exhibit that the MoN-Cu-NPC/CF had the well-preserved morphologies after HER stability test both in 1 M KOH and 0.5 M PBS, further demonstrating the chemical stability for electrolysis. In contrast, the MoN-Cu-NPC/CF after stability in acidic medium displayed obvious particles on the surface, which was the newly formed Cu₂O species obtained by the electrodeposition reaction.

Finally, XPS analysis was applied to observe the chemical bonding of MoN-Cu-NPC/CF after stability test in 1 M KOH. The Mo 3d spectrum still shows a prominent Mo-N bond at 229.7 eV, demonstrating the stability of MoN after test in harsh electrolyte. Besides, two peaks at 232.9 and 232.2 eV for Mo⁴⁺ 3d_{3/2} and Mo⁴⁺ 3d_{5/2} as well as the Mo⁶⁺ 3d_{3/2} peak (235.2 eV) indicated the partial surface oxidation to form the MoO_x species. The Cu 2p spectrum shows two main peaks assigned to Cu 2p_{1/2} and Cu 2p_{3/2} regions, respectively, which was consistent with the original one. The peaks at 952.4 and 932.6 eV could be assigned to Cu(0) derived from the CF substrate. The other two peaks located at 954.4 and 934.6 eV demonstrated the existence of Cu(II) species. Therefore, the MoN-Cu-NPC/CF was highly stable after HER stability test in 1 M KOH.

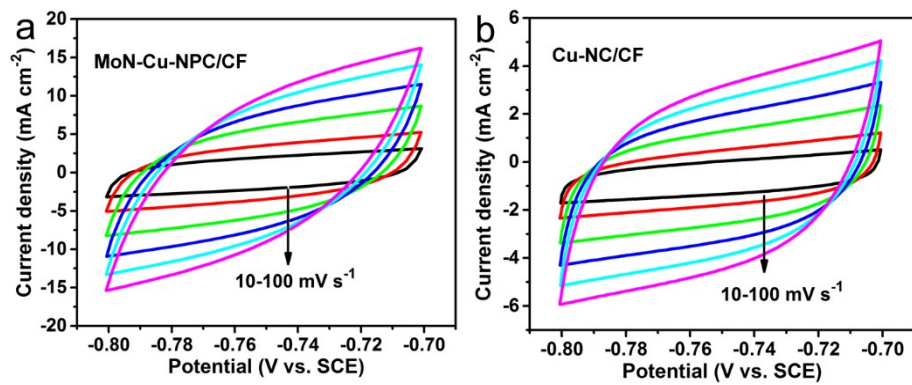


Figure S14. CV curves of (a) MoN-Cu-NPC/CF and (b) Cu-NC/CF ranging from -0.8 to -0.7 V vs. SCE at different scan rates (10-100 mV s⁻¹) in 1 M KOH.

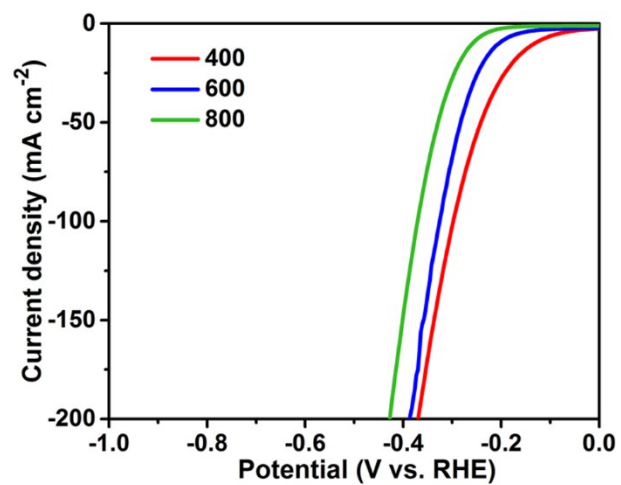


Figure S15. LSV curves of MoN-Cu-NPC/CF prepared at different ammoniation temperatures (400, 600 and 800 °C) in 1 M KOH.

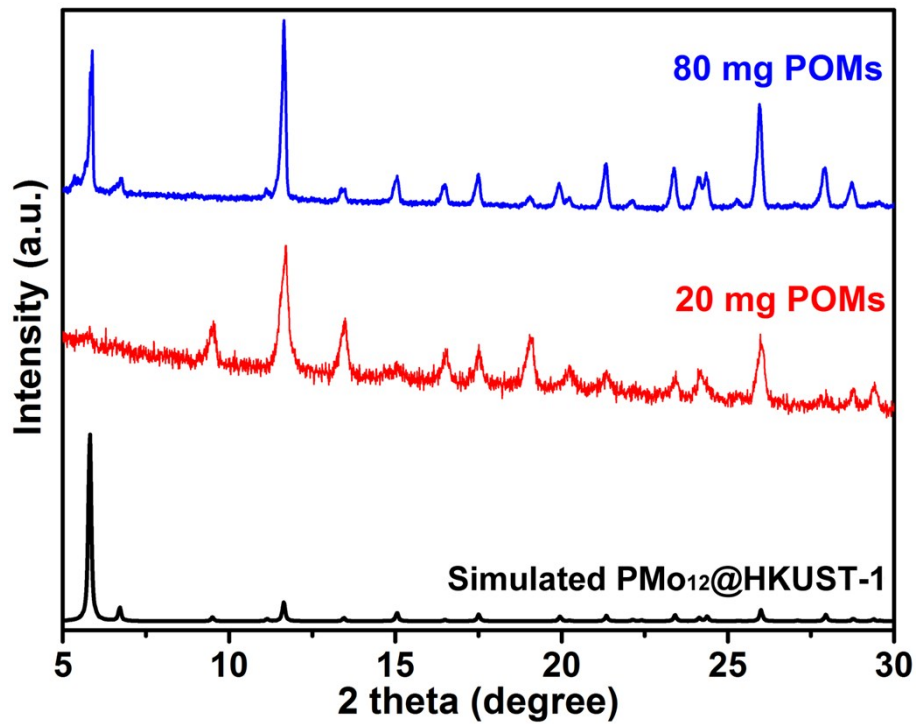


Figure S16. PXRD spectra of PMo₁₂@HKUST-1/CF prepared with different loading amounts of PMo₁₂.

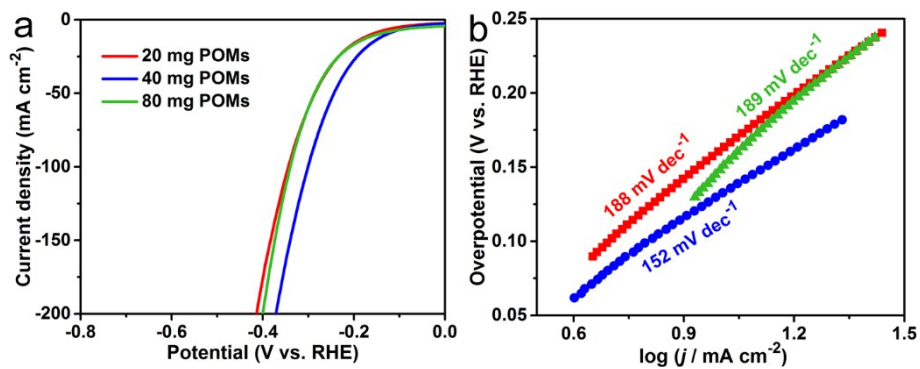


Figure S17. (a) LSV curves and (b) Tafel plots of MoN-Cu-NPC/CF prepared using different POMs in POMOFs/CF precursor in 1 M KOH.

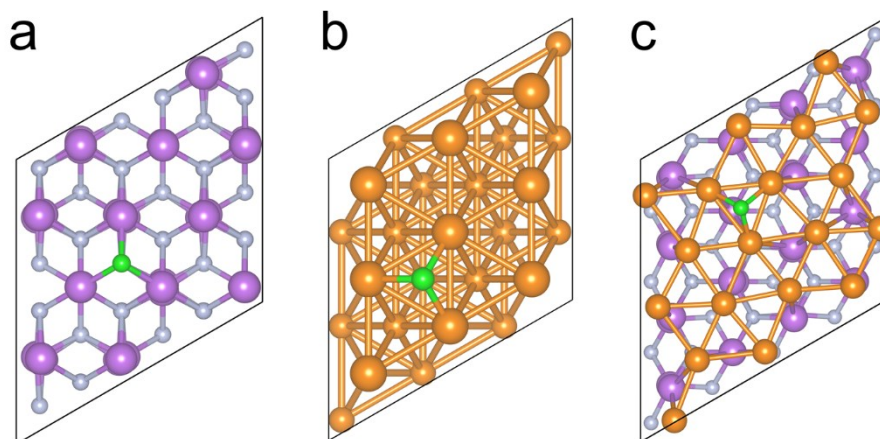


Figure S18. Geometric structures of H* on (a) MoN, (b) Cu and (c) MoN-Cu. Cu, Mo, N, and H are presented by orange, purple, gray, and green spheres, respectively.

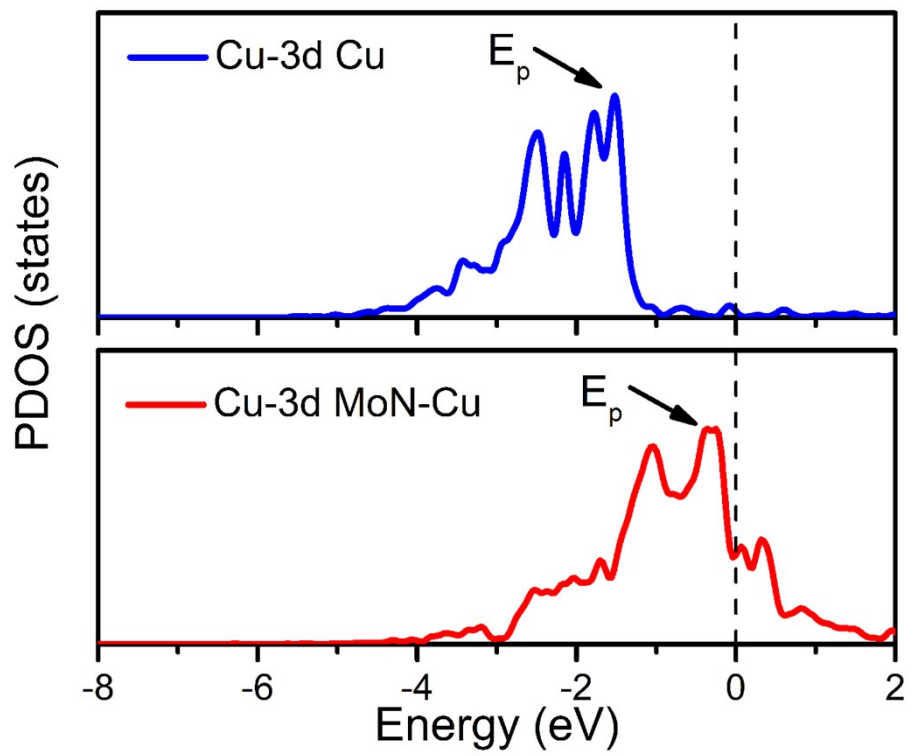


Figure S19. Calculated partial density of states (PDOS) of Cu-3d in Cu and MoN-Cu. The Fermi level is assigned at 0 eV (black dashed lines).

Table S1. Atomic percent (%) of elements in MoN-Cu-NPC/CF according to XPS analysis.

	Mo 3d	Cu 2p	N 1s	P 2p	C 1s	O 1s
MoN-Cu-NPC/CF	4.26	12.41	18.13	2.67	42.99	19.54

Table S2. Comparison of the non-noble metal-based electrocatalysts for HER in different pH-value electrolytes.

Sample	Substrate	Electrolyte	η_{10} (mV vs. RHE)	Tafel slope (mV dec ⁻¹)	Reference
MoN-Cu-NPC/CF	Cu foam	1 M KOH	127	152	This work
		0.5 M H ₂ SO ₄	188	144	
		0.5 M PBS	158	203	
Co _{0.6} Mo _{1.4} N ₂	Glassy carbon	0.1 M HClO ₄	~190	/	[6]
Mo ₂ N/CNT-GR	Glassy carbon	0.5 M H ₂ SO ₄	186	72	[7]
MoN nanosheet	Glassy carbon	0.5 M H ₂ SO ₄	300 mA at 38.5 mA cm ⁻²	90	[8]
γ -Mo ₂ N	Glassy carbon	0.5 M H ₂ SO ₄	381	100	[9]
		1 M KOH	353	108	
Mo ₂ N-MoS ₂	Glassy carbon	0.5 M H ₂ SO ₄	190	59	[10]
WN NW	Carbon cloth	0.5 M H ₂ SO ₄	134	59.6	[11]
		1 M KOH	130	57.1	
Co-Ni ₃ N	Carbon cloth	1 M KOH	194	156	[12]
PVA-Mo ₂ C/Mo ₂ N	Glassy carbon	0.5 M H ₂ SO ₄	132	51.8	[13]
		1 M KOH	142	50.4	
NiS ₂ /MoS ₂ HNW	Glassy carbon	1 M KOH	204	65	[14]
		0.5 M H ₂ SO ₄	235	58	
		0.1 M PBS	284	83	
CoMoS ₄ -H	Glassy carbon	1 M KOH	78	89	[15]

		0.5 M H ₂ SO ₄	170	79.9	
		0.1 M PBS	~520	253.7	
Ni ₂ P	Glassy carbon	1 M KOH	290	47	[16]
FeP NPs@NPC	Glassy carbon	0.5 M H ₂ SO ₄	130	67	[17]
		1 M PBS	386	136	
		1 M KOH	214	82	
Ni-Cu-P	Ni sheets	1 M KOH	120	69	[18]
		0.5 M H ₂ SO ₄	150	/	

Table S3. Calculated zero-point energy correction (E_{ZPE}), entropy contribution (TS), and the total free energy correction ($G_{H^*} - E_{elec}$) of the studied systems.

Species	E_{ZPE} (eV)	$-TS$ (eV)	$G_{H^*} - E_{elec}$ (eV)
H ₂	0.27	-0.41	-0.14
H* on MoN	0.19	0.00	0.19
H* on Cu	0.17	-0.01	0.16
H* on MoN-Cu	0.14	-0.01	0.13

References

- [1] L. Yu, H. Zhou, J. Sun, F. Qin, F. Yu, J. Bao, Y. Yu, S. Chen and Z. Ren, *Energy Environ. Sci.*, 2017, **10**, 1820-1827.
- [2] Y. Li, S. Chang, X. Liu, J. Huang, J. Yin, G. Wang and D. Cao, *Electrochim. Acta*, 2012, **85**, 393-398.
- [3] T. Nosaka, M. Yoshitake, A. Okamoto, S. Ogawa and Y. Nakayama, *Appl. Surf. Sci.*, 2001, **169**, 358-361.
- [4] A. Baiker and M. Maciejewski, *J. Chem. Soc., Faraday Trans. 1*, 1984, **80**, 2331-2341.
- [5] J. A. Switzer, C.-J. Hung, L.-Y. Huang, E. R. Switzer, D. R. Kammler, T. D. Golden and E. W. Bohannon, *J. Am. Chem. Soc.*, 1998, **120**, 3530-3531.
- [6] B. Cao, G.M. Veith, J.C. Neuefeind, R.R. Adzic and P.G. Khalifah, *J. Am. Chem. Soc.*, 2013,

135, 19186-19192.

[7] D.H. Youn, S. Han, J.Y. Kim, J.Y. Kim, H. Park, S.H. Choi and J.S. Lee, *ACS Nano*, 2014, **8**, 5164-5173.

[8] J. Xie, S. Li, X. Zhang, J. Zhang, R. Wang, H. Zhang, B. Pan and Y. Xie, *Chem. Sci.*, 2014, **5**, 4615-4620.

[9] L. Ma, L.R.L. Ting, V. Molinari, C. Giordano and B.S. Yeo, *J. Mater. Chem. A*, 2015, **3**, 8361-8368.

[10] K. Ojha, S. Saha, S. Banerjee and A.K. Ganguli, *ACS Appl. Mater. Interfaces*, 2017, **9**, 19455-19461.

[11] B. Ren, D. Li, Q. Jin, H. Cui and C. Wang, *J. Mater. Chem. A*, 2017, **5**, 19072-19078.

[12] C. Zhu, A.L. Wang, W. Xiao, D. Chao, X. Zhang, N.H. Tiep, S. Chen, J. Kang, X. Wang and J. Ding, *Adv. Mater.*, 2018, **30**, 1705516.

[13] X. Chen, J. Qi, P. Wang, C. Li, X. Chen and C. Liang, *Electrochim. Acta*, 2018, **273**, 239-247.

[14] P. Kuang, T. Tong, K. Fan and J. Yu, *ACS Catal.*, 2017, **7**, 6179-6187.

[15] L. Shao, X. Qian, X. Wang, H. Li, R. Yan and L. Hou, *Electrochim. Acta*, 2016, **213**, 236-243.

[16] L.-A. Stern, L. Feng, F. Song and X. Hu, *Energy Environ. Sci.*, 2015, **8**, 2347-2351.

[17] Z. Pu, I. S. Amiin, C. Zhang, M. Wang, Z. Kou and S. Mu, *Nanoscale*, 2017, **9**, 3555-3560.

[18] M. Cao, Z. Xue, J. Niu, J. Qin, M. Sawangphruk, X. Zhang and R. Liu, *ACS Appl. Mater. Interfaces*, 2018, **10**, 35224-35233